Accurate and efficient calculation of multicomponent thermal diffusion coefficients and partial thermal conductivity based on kinetic theory

Oscar Córdoba[a,*], Manuel Arias-Zugasti[b]

[a] *Escuela Internacional de Doctorado, Universidad Nacional de Educación a Distancia (UNED), Bravo Murillo 38, 28015 Madrid, Spain*

[b] *Departamento de Física Matemática y de Fluidos, Facultad de Ciencias Universidad Nacional de Educación a Distancia (UNED), Av. de Esparta s/n, Carretera de Las Rozas al Escorial km 5, 28232 Las Rozas (Madrid), Spain*

Abstract

The calculation of the multicomponent thermal diffusion coefficients and partial thermal conductivity of polyatomic gas mixtures, with large numbers of components, based on the Kinetic Theory of Gases is revisited. The terms involving inelastic collisions and relaxation times for various internal degrees of freedom are considered, in addition to the classical Chapman-Enskog expressions. For polar gases, the resonant exchange of rotational energy is also accounted for. The present work is the natural extension of the algorithms shown in Combust. and Flame 163 (2016) 540-55 for the calculation of the Fick's law multicomponent diffusion coefficients, of which it makes use.

This work presents a new iterative algorithm for the calculation of the multicomponent thermal diffusion coefficients and partial thermal conductivity. This new algorithm has been implemented in the C++ library MuTLib (Multicomponent Transport Library), available for the transport properties calculations in third party applications and included in the additional material of this publication. The algorithm performance improvements are shown in two different flames: a hydrogen premixed flame and a methane diffusion flame. The results are successfully compared against the library package EGLib (Ern-Giovangigli Library, which considers the same physical effects as this work), and to the well known mixture averaged approximation.

*Corresponding author: ocordoba@dfmf.uned.es

1. Introduction

Diffusion is the transport phenomenon responsible for mixing at the molecular level, playing an important role in combustion [1]. As is well known, diffusion fluxes are proportional to species concentration and temperature gradients, with Fick's law multicomponent diffusion coefficients D_{ij} $(i, j = 1, \ldots, N)$ and thermal diffusion coefficients D_{Ti} being the corresponding respective transport coefficients [2, 3]. Hence, accurate calculation of D_{ij} and D_{Ti} is the key for a correct evaluation of diffusion fluxes in multicomponent mixtures. Once all the relevant physical processes taking place in a typical combustion environment are accurately represented (in particular multicomponent diffusion and chemical kinetics), it is possible to perform Direct Numerical Simulations (DNS) of laminar or turbulent flames, which may be considered as numerical experiments.

In the case of mixtures of dilute gases, the Kinetic Theory of Gases (KTG) [4, 5, 6] provides a general framework for the calculation of the multicomponent diffusion coefficients D_{ij} and D_{Ti}, thermal conductivity and viscosity, based on knowledge on the molecular characteristics of all chemical species in the mixture (i.e., molecular masses, sizes and intermolecular interaction potentials among all different species in the mixture). Classical theory provides very good results on monoatomic gases assuming elastic interactions between molecules. Within the Kinetic Theory of Gases framework and based on the Chapman-Enskog expansion, a step forward was given in reference [7] to account for polar interactions, monopolar-polar interactions, non elastic interaction and polar resonant collisions. Based on this, in references [8, 9, 10], a formal kinetic theory for polyatomic gases was requiring the resolution of a linear system with $3N$ equations (or $2N+P$, where P is the number of non monoatomic molecules). The solution of the aforementioned systems poses no difficulty. However, if the number of components in the mixture is high, the evaluation of the transport properties must be evaluated at every time step and every node in the computational mesh and can become computationally expensive in DNS of unsteady flames. This is because the aforementioned linear systems depend on the mixture composition and temperature. The former difficulty has motivated the development of useful simplified approximations, such as *mixture averaged* transport properties, which becomes quite accurate in the dilute limit, or the use of *constant Lewis numbers*, which is useful in theoretical combustion analyses as it leads to simplified evolution equations [1, 3]. Recent works have tested simplified models using Lewis number in the stabilization effect of premixed flames [11]. In reference [12], the authors show the validation of the mixture averaged approximation in hydrogen flames with thermal diffusion. Nevertheless, a proper evaluation of multicomponent transport properties is critical in accurate DNS of reactive flows. For instance, detailed multicomponent transport can have an important effect in turbulent flames in regions where the front experiences strong curvature [13] and in cases with Reynolds numbers between 600 and 8000 [14].

After the initial studies on multicomponent diffusion in combustion by Dixon-Lewis [15] followed by Jones and Boris [16] and Oran and Boris [17], the general problem of multicomponent transport is addressed by Giovangigli (see, e.g., [18, 19, 20, 21, 22]). In particular, the application of standard iterative methods for the calculation of the transport properties of multicomponent mixtures is investigated in reference [23]. For a review on the implementations for transport calculations available in 2011 see [24]. A different strategy is adopted by Xin et al. in a more recent work [25], based on a *sensitivity analysis* which determines the group of species whose diffusive transport has strongest impact on flame dynamics, thus allowing for a simplified treatment of the transport properties of the remaining species.

The calculation of the multicomponent Fick diffusion coefficients was also analyzed by Arias-Zugasti et al. [26], where two efficient new algorithms: Model 1 and Model 1+M, are derived for the calculation of D_{ij}. The optimal implementation of Model 1+M was subsequently analyzed by Naud and Arias-Zugasti [27]. In Model 1, based on [28], the multicomponent mixture is assumed to be dilute in 1 major species, and D_{ij} is given as a power series in terms of the remaining $N-1$ mole fractions in the mixture. As a natural extension of Model 1, in Model 1+M the mixture is assumed to contain a total of $1+M$ major species, and D_{ij} are computed as a power series in terms of the remaining $N-M-1$ mole fractions, which are assumed to be close to the dilute limit, thus avoiding the use of approximate methods regarding the major, non-dilute, species.

The purpose of this work is to provide a new simple, efficient and accurate iterative algorithm for the evaluation of the multicomponent thermal diffusion coefficients and partial thermal conductivity of typical combustion gas mixtures. The general idea to achieve this goal is to formulate the problem in terms of dimensionless variables, based on the correct characteristic scales, in a similar way as it is done for Model 1 of [26] for the calculation of D_{ij}. As shown below, the proposed solution makes use of the results shown in [26] and involves a new linear system of equations resolution with sub-matrices which are diagonally dominant, thus allowing for an efficient inversion based on the Neumann series.

The proposed algorithm has been implemented in the C++ library MuTLib, included as additional material. The results are presented for a premixed hydrogen flame and a diffusion methane flame and compared against mixture averaged thermal diffusion and the software library package EGLib, developed by Ern and Giovangigli [23]. The level of accuracy vs. number of iterations is shown to probe the algorithm efficiency.

2. Mass conservation and heat equation in multicomponent gases

In the present work we consider a multicomponent ideal gas mixture with N different chemical species, assuming that all state variables in the mixture are given quantities (mass

density ρ, molecular number density n, pressure p and absolute temperature T). Following the notation of [6], the mole fraction of species i will be denoted by $x_i = n_i/n$, and the mass fraction of species i by $y_i = \rho_i/\rho$, where n_i is the molecular number density of species i and ρ_i is the local mass density of species i. Mole and mass fractions are related by $m_i x_i = m y_i$, where m_i is the *molecular* mass of species i and m is the *molecular* mass of the mixture, given by the corresponding *mole* mass over Avogadro's number.

2.1. Mass conservation equations in multicomponent gases

As is well known, the macroscopic mass conservation equations in a multicomponent mixture are given by (see, e.g., [1, 2, 3])

$$\frac{1}{\rho_i}\frac{d\rho_i}{dt} = -\nabla\cdot(\mathbf{v}+\mathbf{V}_i) - \frac{1}{\rho_i}\mathbf{V}_i\cdot\nabla\rho_i; \qquad i = 1,\ldots,N \tag{1}$$

where $\mathbf{v}$ is the mixture hydrodynamic velocity , $\dfrac{d}{dt}$ stands for the substantial derivative $\dfrac{d}{dt} = \dfrac{\partial}{\partial t} + \mathbf{v}\cdot\nabla$ and $\mathbf{V}_i$ are the diffusion velocities, with

$$\sum_i \rho_i \mathbf{V}_i = 0 \tag{2}$$

The former conservation equations can be easily derived from the macroscopic point of view, by imposing the mass conservation principle in the continuum approximation. On the other hand, Eq. (1) can also be derived from the microscopic (i.e., molecular) point of view, accounting for the mass as collision invariant in the Boltzmann equation [6]. In this regard, following the Kinetic Theory of Gases, the Chapman-Enskog method determines successive approximations to the solution of the Boltzmann equation. Zero order approximation leads to Euler hydrodynamic equations while the first order approximation leads to the Navier-Stokes equations. Kinetic Theory of Gases is more than a mathematical way to get the proper conservation equations, as it also leads to the correct expressions for the molecular transport fluxes (of momentum, mass and energy) and provides a model based on first principles which allows for the calculation of the corresponding molecular (i.e., diffusive) transport coefficients, based on basic descriptions of individual particles and their collisions behavior. For instance, the first Chapman-Enskog order mass conservation equation terms are

$$\mathbf{V}_i = -\sum_j D_{ij}\mathbf{d}_j - D_{Ti}\nabla\ln T \tag{3}$$

where D_{ij} are the multicomponent diffusion coefficients, D_{Ti} are the multicomponent thermal diffusion coefficients, $\mathbf{d}_i$ are the mass diffusion driving force vectors, given by

$$\mathbf{d}_i = \nabla x_i + (x_i - y_i)\nabla \ln p - \frac{\rho y_i}{p}\left(\mathbf{F}_i - \sum_j y_j \mathbf{F}_j\right) \tag{4}$$

and where $\mathbf{F}_i$ is the body force per unit mass acting on species i. As can be seen, the first term in Eq. (3) provides the contribution to the mass diffusion of species i due to composition inhomogeneities in the mixture, barodiffusion and differential external forces, given by the generalized Fick's law. The second term in Eq. (3) is the thermal diffusion, i.e., the diffusive transport of mass as a consequence of a temperature gradient (also known as *thermodiffusion*, *thermophoresis* or *Ludwig–Soret transport*), with corresponding mass fluxes given by

$$\mathbf{j}_{Ti} = -\rho y_i D_{Ti} \nabla \ln T \tag{5}$$

2.2. Heat equation in multicomponent mixtures

As is well known, the calculation of the thermal diffusion coefficients and the partial thermal conductivity according to the KTG are very closely related, thus allowing for a joint framework for the calculation of both transport properties, as shown below. Reference [10] studies the energy equation and heat transmission in polyatomic gas mixtures. The heat flux vector derived from the KTG is

$$\mathbf{q} = k_B T \sum_{i=1}^{N}\left(\frac{5}{2} + \bar{\epsilon}_i\right) n_i \mathbf{V}_i - \lambda' \nabla T - n k_B T \sum_{i=1}^{N} D_{Ti}\mathbf{d}_i \tag{6}$$

where k_B is the Boltzmann constant, $\bar{\epsilon}_i = \dfrac{\sum_{j=1}^{N} \epsilon_{ij} e^{-\epsilon_{ij}}}{\sum_{j=1}^{N} e^{-\epsilon_{ij}}}$, λ' is the partial coefficient of thermal conductivity and the parameter ϵ is the Lennard Jones potential well depth (further discussion about the values ϵ_{ij} may be found in Appendix B from additional material).
The relation between the thermal conductivity λ and the partial thermal conductivity λ' is

$$\lambda = \lambda' - \frac{p}{T}\sum_{i=1}^{N} k_{Ti} D_{Ti} \tag{7}$$

where k_T is the thermal diffusion ratio defined by (8).

$$D_{Ti} = \sum_{j=1}^{N} D_{ij} k_{Tj} \qquad i = 1, \ldots, N$$
$$\sum_{i=1}^{N} k_{Ti} = 0 \tag{8}$$

2.3. Calculation of the transport coefficients according to the KTG

The Kinetic Theory of Gases provides expressions for the evaluation of the molecular transport properties of multicomponent mixtures of dilute gases. Thermal diffusion is often referred to as a *second order* effect. This is because if the zero order is considered in the Chapman-Enskog expansion, the resultant homogeneous system leads to the trivial solution for $[D_{Ti}]_{(0)}$, so at least the first correction in the Chapman-Enskog expansion must be used. The multicomponent thermal diffusion coefficients $[D_{Ti}]_{(1)}$ resultant from the Kinetic Theory of Gases for polyatomic gases are given by

$$[D_{Ti}]_{(1)} = \frac{8}{5} \frac{a_{i,00}^{(1)}}{n k_B} \tag{9}$$

The parameter λ' is obtained in terms of the coefficients $a_{10i}^{(1)}$ and $a_{01i}^{(1)}$, (see Eq. (31) of [15]).

$$\lambda' = -4 \sum_{i=1}^{N} x_i \left(a_{10i}^{(1)} + a_{01i}^{(1)} \right) \tag{10}$$

The values $a_{i,00}^{(1)}$, $a_{10i}^{(1)}$ and $a_{01i}^{(1)}$ are the coefficients of the probability density function (PDF) in the Boltzmann equation written in terms of the Sonine polynomials $S_{\nu}^{(n)}(x)$ (AKA generalized Laguerre polynomials):

$$S_{\nu}^{(n)}(x) = \sum_{p=0}^{n} \frac{\Gamma(\nu + n + 1)}{(n-p)! p! \Gamma(\nu + p + 1)} \tag{11}$$

Assuming a small deviation from the equilibrium PDF in the Boltzmann equation, the KTG computes the transport properties of the system in terms of the aforementioned coefficients by means of a variational procedure (see, e.g., [29] for further details), which leads to the following linear system for $a_{i,00}^{(1)}$, $a_{10i}^{(1)}$ and $a_{01i}^{(1)}$ (see Eq. (24a) of [15])

$$\sum_{j=1}^{N} \sum_{mn} L_{ij}^{rs,mn} a_{j,mn}^{(1)} = (\delta_{r1} + \delta_{s1}) x_i; \qquad \begin{matrix} i = 1, \ldots, N \\ rs, mn = 00, 10, 01 \end{matrix} \tag{12}$$

together with the compatibility condition Eq. (13)

$$\sum_{j=1}^{N} y_j a_{00j}^{(1)} = 0 \Rightarrow \frac{\Lambda_{ii}^{00,00}}{m_i x_i} \sum_{j=1}^{N} m_j x_j a_{00j}^{(1)} = 0 \tag{13}$$

In the present work, instead of the L parameters shown in (12), Λ values are used, consistent with the notation used in reference [6]. The relation between both sets of parameters is given by

$$\begin{aligned} L_{ij}^{00,00} &= 4\left(\tfrac{m_j x_j}{m_i x_i}\Lambda_{ii}^{00,00} - \Lambda_{ij}^{00,00}\right) \\ L_{ij}^{00,10} &= -4\Lambda_{ij}^{00,10} = L_{ji}^{10,00} = -4\Lambda_{ji}^{10,00} \\ L_{ij}^{10,01} &= -4\Lambda_{ij}^{10,01} = L_{ji}^{01,10} = -4\Lambda_{ji}^{01,10} \;; \qquad i,j = 1,\ldots,N \\ L_{ij}^{10,10} &= -4\Lambda_{ij}^{10,10} \\ L_{ij}^{01,01} &= -4\Lambda_{ij}^{01,01} \end{aligned} \tag{14}$$

As can be seen, the difference between L and Λ parameters is a factor of -4 except for the super indexes $00,00$, in which case the relation is given by the former linear combination. The previous system of equations Eq. (12) may be written as:

$$-4\begin{bmatrix} \Lambda^{00,00} & \Lambda^{00,10} & 0 \\ \Lambda^{10,00} & \Lambda^{10,10} & \Lambda^{10,01} \\ 0 & \Lambda^{01,10} & \Lambda^{01,01} \end{bmatrix} \begin{Bmatrix} \mathbf{a}_{00}^{(1)} \\ \mathbf{a}_{10}^{(1)} \\ \mathbf{a}_{01}^{(1)} \end{Bmatrix} = \begin{Bmatrix} 0 \\ \mathbf{x} \\ \mathbf{x} \end{Bmatrix} \tag{15}$$

supplemented by Eq. (13), where vector $\mathbf{a}_{00}^{(1)}$ (with components $a_{i,00}^{(1)}$, $i = 1,\ldots,N$) , $\mathbf{a}_{10}^{(1)}$ (with components $a_{i,10}^{(1)}$, $i = 1,\ldots,N$) and $\mathbf{a}_{01}^{(1)}$ (with components $a_{i,01}^{(1)}$, $i = 1,\ldots,N$) are the N dimensional vectors related to thermal transport properties in the Chapman-Enskog expansion, modified for polyatomic gases, and where vector $\mathbf{x}$ contains the mole fractions x_i.

In general, the coefficients $\Lambda_{ij}^{rs,mn}$ in Eq. (15) are given by mole fraction weighted sums of several microscopic properties of the chemical species in the mixture (see [10]), depending on the molecular sizes, masses, elastic collision integrals—defined in terms of the corresponding interaction potentials, specific molecular heat, inelastic collision parameters and resonant self diffusion parameters. As a consequence, these coefficients depend on mixture composition and temperature. These Λ coefficients can be written in terms of the well known *binary* diffusion coefficients ($\mathscr{D}_{ij}$)

$$\mathscr{D}_{ij} = \frac{3}{8n\sigma_{ij}^2\Omega_{ij}^{(1,1)*}}\left(\frac{k_B T}{2\pi m_{ij}}\right)^{1/2} \tag{16}$$

by means of

$$\Lambda_{ij}^{rs,mn} = \frac{4}{25 k_B n} \sum_{\ell=1}^{N} \frac{x_i x_\ell}{\mathscr{D}_{i\ell}} F_{ij\ell}^{rs,mn}; \qquad rs,mn = 00,10,01 \tag{17}$$

where σ_{ij} is the differential collision cross-section of chemical species i and j, $m_{ij}^{-1} = m_i^{-1} + m_j^{-1}$ denotes the reduced mass and where the reduced collision integrals $\Omega_{ij}^{(1,1)*}$ are tabulated in reference [8]. In the former expression Eq. (17) the dimensionless functions $F_{ij\ell}^{rs,mn}$ depend on temperature, but not on mixture composition, and the details are described in Appendix B from additional material.

3. Derivation of an efficient algorithm for the calculation of the multicomponent thermal diffusion coefficients and partial thermal conductivity according to KTG

The main idea behind the present algorithm for the calculation of the thermal diffusion coefficients has two parts. On one hand inspection of Eq. (15) shows that the coefficient matrix in the first block in this linear system (i.e., $\Lambda^{00,00}$ supplemented by Eq. (13)) is the same matrix that has to be inverted for the calculation of the Fick diffusion coefficients D_{ij}. Thus, the first part of the present algorithm is to solve Eqs. (13, 15) using the blockwise matrix inversion formula

$$\left(\begin{array}{c|c} \mathbf{A} & \mathbf{B} \\ \hline \mathbf{C} & \mathbf{D} \end{array}\right)^{-1} = \left(\begin{array}{c|c} \mathbf{A}^{-1} + \mathbf{A}^{-1}\mathbf{B}(\mathbf{D}-\mathbf{C}\mathbf{A}^{-1}\mathbf{B})^{-1}\mathbf{C}\mathbf{A}^{-1} & -\mathbf{A}^{-1}\mathbf{B}(\mathbf{D}-\mathbf{C}\mathbf{A}^{-1}\mathbf{B})^{-1} \\ \hline -(\mathbf{D}-\mathbf{C}\mathbf{A}^{-1}\mathbf{B})^{-1}\mathbf{C}\mathbf{A}^{-1} & (\mathbf{D}-\mathbf{C}\mathbf{A}^{-1}\mathbf{B})^{-1} \end{array}\right) \tag{18}$$

which holds for any square matrix with entries **A**, **B**, **C**, **D**, as long as sub-matrices **A** and $\mathbf{D}-\mathbf{C}\mathbf{A}^{-1}\mathbf{B}$ are non-singular. In the present case, according to Eq. (15), the sub-matrices **A**, **B**, **C**, **D** are defined by

$$\mathbf{A} = \Lambda^{00,00} \tag{19}$$

$$\mathbf{B} = \left[\begin{array}{cc} \Lambda^{00,10} & 0 \end{array}\right] \tag{20}$$

$$\mathbf{C} = \left[\begin{array}{c} \Lambda^{10,00} \\ 0 \end{array}\right] \tag{21}$$

$$\mathbf{D} = \left[\begin{array}{cc} \Lambda^{10,10} & \Lambda^{10,01} \\ \Lambda^{01,10} & \Lambda^{01,01} \end{array}\right] \tag{22}$$

In the application of this strategy to the linear system under consideration the inverse of the first block ($\Lambda^{00,00}$ supplemented by Eq. (13), **A** in Eq. (18)) is already available from

the calculation of D_{ij}. The second part of the algorithm makes use of the observation that the second block that needs to be inverted to solve Eq. (15), i.e., $\mathbf{D}-\mathbf{C}\mathbf{A}^{-1}\mathbf{B}$ in Eq. (18), is diagonally dominant. Hence, by scaling this part of the system (blocks $\Lambda^{10,00}$, $\Lambda^{10,10}$, $\Lambda^{10,01}$, $\Lambda^{01,10}$and $\Lambda^{01,01}$) with the corresponding diagonal terms, the block $\mathbf{D}-\mathbf{C}\mathbf{A}^{-1}\mathbf{B}$ is written as $\mathbb{1}+A_T$ (see Eq. (35) below) and its inverse can be efficiently computed by means of the Neumann series [30] (i.e., the matrix version of the geometric series)

$$(\mathbb{1}+A_T)^{-1}_{ij}=\left(\sum_{r=0}^{\infty}(-A_T)^r\right)_{ij} \tag{23}$$

which is convergent as long as the norm of matrix A_T is $\|A_T\|<1$, and has fast convergence rate if $\|A_T\|\ll 1$ (where we define matrix A_T, Eq. (35), by analogy with matrix A in Model 1 of [26]). This way the present algorithm makes full use of the information available from the calculation of the Fick diffusion coefficients D_{ij}, which is assumed to have been performed prior to the calculation of the thermal diffusion coefficients. On the other hand, the solution for D_{Ti} is written in terms of a Neumann series, in a similar way as it is done in Model 1 of [26]. The implementation of this general strategy is shown in full detail below.

3.1. Final expression for the KTG linear system

The system of equations (15) may be scaled according to the following expressions:

$$\begin{aligned} F_{ij}^{rs,mn} &= \lambda_i^{rs}\mu_j^{mn}\frac{25k_Bn}{4}\Lambda_{ij}^{rs,mn} \\ \tilde{a}_{mnj} &= -\frac{8}{5nk_B}\frac{a_{mnj}^{(1)}}{\mu_j^{mn}} \qquad ; \qquad i,j=1,\ldots,N \\ \tilde{x}_{rsi} &= \frac{5}{2}\lambda_i^{rs}x_i \end{aligned} \tag{24}$$

with:

$$\lambda_i^{00}=1 \qquad \lambda_i^{10}=\frac{x_i}{\frac{25k_Bn}{4}\Lambda_{ii}^{10,10}\mathscr{D}_{ii}} \qquad \lambda_i^{01}=\frac{x_i\left(\frac{c_{i,\text{int.}}}{k_B}\right)}{\frac{25k_Bn}{4}\Lambda_{ii}^{01,01}\left(\frac{c_{i,\text{int.}}}{k_B}\right)^2\mathscr{D}_{ii}} \qquad i=1,\ldots,N; \tag{25}$$

$$\mu_j^{00}=\frac{\mathscr{D}_{jN}}{x_j} \qquad \mu_j^{10}=\frac{\mathscr{D}_{jj}}{x_j} \qquad \mu_j^{01}=\frac{\mathscr{D}_{jj}\left(\frac{c_{j,\text{int.}}}{k_B}\right)}{x_j} \qquad j=1,\ldots,N; \tag{26}$$

where $c_{i,int}$ is the internal component of the molecular heat capacities for the species i (further details in Appendix B from additional material). The reference species N has been selected as the species with highest mole fraction, in the same way as it is done in Model 1 and Model 1+M of [26]. This way we are able to make use of the results available from the calculation of D_{ij}. On the other hand, based on the observation that the second block in Eq. (15) is diagonally dominant, instead of using the reference species N to define the dimensionless variables, the reference scales in this part of the system are given by the corresponding diagonal terms. Note that the factor $\dfrac{1}{x_j}$ above is just a way to write the equations in a compact way, i.e., from the computational point of view, there is no division by magnitudes close to zero for vanishing molar fractions[1]. Note also that for convenience the expressions $\dfrac{25k_Bn}{4}\Lambda_{ii}^{10,10} = \displaystyle\sum_{\ell=1}^{N}\frac{x_ix_\ell}{\mathscr{D}_{i\ell}}F_{ij\ell}^{10,10}$ and $\dfrac{25k_Bn}{4}\Lambda_{ii}^{01,01}\left(\dfrac{c_{i,\text{int.}}}{k_B}\right)^2 = \displaystyle\sum_{\ell=1}^{N}\frac{x_ix_\ell}{\mathscr{D}_{i\ell}}\left(\frac{c_{i,\text{int.}}}{k_B}\right)^2 F_{ij\ell}^{01,01}$ have been used.

Inserting the former definitions in Eq. (15), the KTG linear system is written in dimensionless form as

$$\begin{bmatrix} F^{00,00} & F^{00,10} & 0 \\ F^{10,00} & F^{10,10} & F^{10,01} \\ 0 & F^{01,10} & \mathbb{1} \end{bmatrix} \begin{Bmatrix} \tilde{\mathbf{a}}_{00} \\ \tilde{\mathbf{a}}_{10} \\ \tilde{\mathbf{a}}_{01} \end{Bmatrix} = \begin{Bmatrix} \mathbf{0} \\ \tilde{\mathbf{x}}_{10} \\ \tilde{\mathbf{x}}_{01} \end{Bmatrix} \tag{27}$$

where the resultant last $2\times N$ equations have been scaled with the diagonal terms to improve the convergence rate of the Neumann series used in the inversion of this part of the system. Note that for monoatomic species $c_{i,\text{int.}} = 0$ and the correspondent equation $\sum_{j=1}^{N-1} F_{ij}^{01,10}\tilde{a}_{10j} + \tilde{a}_{01i} = \tilde{x}_{01i}$ only makes sense if $\tilde{a}_{01i} = 0$. In this case there are two options: direct elimination of the former equations from system (27) or make them compatible with (28) by means of

$$\begin{aligned} F_{ij}^{10,01} &= 0 \\ F_{ij}^{01,01} &= \delta_{ij} \text{ for monoatomic species} \\ \tilde{x}_{01i} &= 0 \end{aligned} \tag{28}$$

Before using the blockwise inversion formula Eq. (18), the N^{th} equation in the linear

[1]Taking into account the nature of expressions F_{ijl} described in Appendix B from additional material, the resultant expressions related to the molar fractions are $\dfrac{x_ix_\ell}{x_j}\delta_{ij}$ and $\dfrac{x_ix_\ell}{x_j}\delta_{jl}$. In the first case $\dfrac{x_ix_\ell}{x_j}\delta_{ij} = x_l$ if $i = j$ and zero otherwise. As well, $\dfrac{x_ix_\ell}{x_j}\delta_{jl} = x_i$ if $j = l$ and zero otherwise.

system Eq. (27) (i.e., the last equation in the first block, which can be expressed as a linear combination of the $N-1$ previous equations) is substituted by the overall mass conservation condition Eq. (13), which is used to calculate the last entry of vector $\tilde{\mathbf{a}}_0$. This way the present calculation strategy ensures exact mass conservation not only for the converged results, but also for the approximate results found at any finite iteration level of the present algorithm. Thus we find

$$\tilde{a}_{00N} = -\sum_{j=1}^{N-1} \frac{m_j}{m_N} \frac{\mathscr{D}_{jN}}{\mathscr{D}_{NN}} \tilde{a}_{00j} \tag{29}$$

and we define vector $\tilde{\mathbf{a}}_{00}^{-}$ as the vector containing the remaining values $\tilde{a}_{00j}$:

$$\tilde{a}_{00i}^{-} = \tilde{a}_{00i}; \qquad i = 1,\ldots,N-1 \tag{30}$$

Inserting this last result in Eq. (27), the KTG linear system for the thermal diffusion coefficients is finally written as Eq. (31)

$$\begin{bmatrix} \mathbb{1}+A & F^{00,10} & 0 \\ \hat{F}^{10,00} & F^{10,10} & F^{10,01} \\ 0 & F^{01,10} & \mathbb{1} \end{bmatrix} \begin{Bmatrix} \tilde{\mathbf{a}}_{00}^{-} \\ \tilde{\mathbf{a}}_{10} \\ \tilde{\mathbf{a}}_{01} \end{Bmatrix} = \begin{Bmatrix} \mathbf{0}^{-} \\ \tilde{\mathbf{x}}_{10} \\ \tilde{\mathbf{x}}_{01} \end{Bmatrix} \tag{31}$$

where

$$A_{ij} = F_{ij}^{00,00} - \frac{m_j}{m_N} \frac{\mathscr{D}_{jN}}{\mathscr{D}_{NN}} F_{iN}^{00,00} - \delta_{ij}; \qquad i,j = 1,\ldots,N-1 \tag{32}$$

$$\hat{F}_{ij}^{10,00} = F_{ij}^{10,00} - \frac{m_j}{m_N} \frac{\mathscr{D}_{jN}}{\mathscr{D}_{NN}} F_{iN}^{10,00}; \qquad i = 1,\ldots,N; \qquad j = 1,\ldots,N-1 \tag{33}$$

Eq. (31) is the final expression for the KTG linear system for D_{Ti} and λ'. The solution of this system can be computed by means of the blockwise inversion formula Eq. (18). In this regard, the first sub-matrix that needs to be inverted is $\mathbb{1}+A$, where, as can be easily checked, A_{ij} (defined in Eq. (32)) is the same matrix A_{ij} given by Eq. (21) of [26]. Thus, the inverse of this block is already known from the calculation of the Fick diffusion coefficients (see Eq. (20) of [26]), since we are assuming that the calculation of D_{ij} has been completed prior to the calculation of D_{Ti} and λ'.

3.2. Solution of the second block and expressions for the multicomponent thermal diffusion coefficients and partial thermal conductivity

According to the scaling used to derive Eq. (31), the new block matrix to be inverted using the blockwise matrix inversion formula (18) can be written as:

$$\left[D-CA^{-1}B\right]^{-1}=\left[\begin{array}{cc}\left(\mathbb{1}+A_T\right)^{-1} & -\left(\mathbb{1}+A_T\right)F^{10,01}\\ -F^{01,10}\left(\mathbb{1}+A_T\right)^{-1} & \mathbb{1}+F^{01,10}\left(\mathbb{1}+A_T\right)^{-1}F^{10,01}\end{array}\right] \tag{34}$$

where, by analogy with matrix A in Model 1 of [26], we define matrix A_T by means of

$$\mathbb{1}+A_T=F^{10,10}-\hat{F}^{10,00}\left(\mathbb{1}+A\right)^{-1}F^{00,10}-F^{10,01}F^{01,10} \tag{35}$$

Since this matrix is close to the identity it is reasonable to expect that the Neumann series inversion formula (Eq. (23)) can be used to define an approximate iterative algorithm with fast convergence rate. With this idea in mind, the thermal diffusion coefficients are given by means of

$$\left\{\ \tilde{\mathbf{a}}_{00}^{-}\ \right\}=\left(\mathbb{1}+A\right)^{-1}F^{00,10}\left(\mathbb{1}+A_T\right)^{-1}\left(F^{10,01}\tilde{\mathbf{x}}_{01}-\tilde{\mathbf{x}}_{10}\right) \tag{36}$$

where $\left(\mathbb{1}+A\right)^{-1}$ is known from the calculation of the Fick diffusion coefficients and where $\left(\mathbb{1}+A_T\right)^{-1}$ can be computed in an iterative fashion using the Neumann series Eq. (23). For instance, to leading order (i.e., for $r=0$) $\left(\mathbb{1}+A_T\right)^{-1}=\mathbb{1}$, whereas the first term ($r=1$) would give $\left(\mathbb{1}+A_T\right)^{-1}=\mathbb{1}-A_T$. Note that the first iteration does not involve matrix multiplications.
Finally, the thermal diffusion coefficients can be easily calculated from the former result recalling Eqs. (9, 25, 26, 29). On the other hand, the thermal diffusion fluxes can be directly computed by means of

$$\mathbf{j}_{Ti}=-\rho\frac{m_i}{m}\mathscr{D}_{iN}\tilde{a}_{00i}\nabla\ln T \tag{37}$$

The coefficients $a_{10i}^{(1)}$ and $a_{01i}^{(1)}$ may be derived from the scaled parameters $\tilde{a}_{10i}$ and $\tilde{a}_{01i}$ that may be computed using the expressions:

$$\left\{\ \tilde{\mathbf{a}}_{10}\ \right\}=-\left(\mathbb{1}+A_T\right)^{-1}\left(F^{10,01}\tilde{\mathbf{x}}_{01}-\tilde{\mathbf{x}}_{10}\right) \tag{38}$$

$$\left\{\ \tilde{\mathbf{a}}_{01}\ \right\}=\tilde{\mathbf{x}}_{01}+F^{01,10}\left(\mathbb{1}+A_T\right)^{-1}\left(F^{10,01}\tilde{\mathbf{x}}_{01}-\tilde{\mathbf{x}}_{10}\right) \tag{39}$$

It will be noted that aforementioned matrix inversion $\left(\mathbb{1}+A\right)^{-1}$ is not strictly needed to obtain the vectors $\left\{\ \tilde{\mathbf{a}}_{00}^{-}\ \right\}$, $\left\{\ \tilde{\mathbf{a}}_{10}\ \right\}$ and $\left\{\ \tilde{\mathbf{a}}_{01}\ \right\}$ with a desired level of convergence. From the computational point of view it is more efficient to simply implement algorithms with successive matrix-vectors multiplications, see Figure 1. For that purpose the expressions (35) and (23) must be taken into account.

$\mathbf{v}_1 = F^{10,01}\tilde{\mathbf{x}}_{01}$
$\mathbf{w} = \tilde{\mathbf{x}}_{10} - \mathbf{v}_1$
$\tilde{\mathbf{a}}_{10} = \mathbf{w}$

loop for the number of iterations
$\mathbf{v}_1 = F^{01,10}\mathbf{w}$
$\mathbf{v}_2 = F^{10,01}\mathbf{v}_1$
$\mathbf{v}_3 = F^{00,10}\mathbf{w}$
$\mathbf{v}_4 = (\mathbb{1} + A)^{-1}\,\mathbf{v}_3$
$\mathbf{v}_1 = \hat{F}^{10,00}\mathbf{v}_4$
$\mathbf{v}_5 = F^{10,10}\mathbf{w}$
$\mathbf{w} = \mathbf{v}_1 + \mathbf{v}_2 - \mathbf{v}_5 + \mathbf{w}$
$\tilde{\mathbf{a}}_{10} = \tilde{\mathbf{a}}_{10} + \mathbf{w}$
end of the loop

$\tilde{\mathbf{a}}_{01} = F^{01,10}\tilde{\mathbf{a}}_{10}$
$\tilde{\mathbf{a}}_{01} = \tilde{\mathbf{x}}_{01} - \tilde{\mathbf{a}}_{01}$
$\mathbf{v}_3 = F^{00,10}\tilde{\mathbf{a}}_{\mathbf{10}}$
$\tilde{\mathbf{a}}^{-}_{00} = -(\mathbb{1} + A)^{-1}\,\mathbf{v}_3$

Figure 1: Algorithm scheme for the calculation of vectors $\tilde{\mathbf{a}}^{-}_{00}$, $\tilde{\mathbf{a}}_{10}$ and $\tilde{\mathbf{a}}_{01}$ as matrix-vector multiplications

3.3. Transport algorithm implementation and validation

The presented methodology and the algorithms from [26] have been implemented and tested in the C++ library MuTLib, and the corresponding results have been compared against the Fortran package EGLib [31, 23]. It is important to remark that both packages (MuTLib and EGLib) consider the same physical effects included in the full multicomponent transport description available in the Chemkin package [32]. Therefore, a gas mixture with the same inputs leads to equivalent systems of linear equations for the transport properties evaluation and a direct inversion produces the same results.

Both packages deploy the transport magnitudes (Fick diffusion coefficients, thermal diffusion coefficients and partial thermal conductivity) for a given temperature and mixture molar fractions. To this end, MuTLib is able to read and interpolate the thermodynamic data (specific heat), the kinetic data (collision diameter, rotational collision index, Lennard Jones potential, etc.) and the collision integral tables for interpolation and evaluation as a function of mixture composition and temperature. On the other hand, EGLib expects more elaborated inputs, such us binary diffusion coefficients, collision integrals A^*, B^*, C^*, viscosity and collision integrals as polynomials of temperature for the species involved in the mixture. EGLib also expects the specific heat as a direct input to the user subroutines and assumes that the expressions for resonant exchange of internal energy are embedded in the supplied binary diffusion coefficients.

Regarding the iteration level, MuTLib may be executed with different degrees of iteration separately for the Fick diffusion coefficients and the partial thermal conductivity. On the other hand EGLib only provides the options of either using direct inversion or a predefined set of conjugate gradient iterations (i.e., three iterations for the thermal diffusion vector and thermal conductivity, the last one preconditioned and two iterations for the Fick diffusion coefficients).

3.4. Algorithm efficiency

The number of operations implied in the present algorithm is addressed below. It will be compared against other well known algorithms, including a direct LDL^T and two iterative conjugate gradient algorithms, with and without preconditioning. It will be assumed that the matrix system and the right hand side of the linear system are given. No considerations are done about the operations needed to build the linear system of equations, only the number of operations needed to reach the solution is accounted for. The approach is very generic and the numbers of operations are estimated approximately, although minor order numbers of operations will be kept. Any of the algorithms used for comparison may be optimized or customized for the current problem and the number of operations may differ slightly. Thus, the main purpose here is only to provide a general idea of the algorithm cost in terms of the different numbers of additions and multiplications needed in each case.

For instance, for preconditioning we have considered a left matrix-vector multiplication, where a dense preconditioning matrix is assumed and no sparsity issues are taken into account.

The sequence of matrix-vector multiplications in (38) $(\mathbb{1}+A_T)^{-1}\left(\tilde{\mathbf{x}}_{10}-F^{10,01}\tilde{\mathbf{x}}_{01}\right)$ are repeated in the expressions (36) and (39) from right to left. A single matrix-vector multiplication of order N takes $MV = 2N^2 - N$ operations. The computation of the vector $F^{10,01}\tilde{\mathbf{x}}_{01} - \tilde{\mathbf{x}}_{10}$ requires $N + MV$ operations. Taking into account the expression (35), the resultant vector $-(\mathbb{1}+A_T)\left(F^{10,01}\tilde{\mathbf{x}}_{01} - \tilde{\mathbf{x}}_{10}\right)$ requires ca. $7MV + 4N$ operations. The value is approximated because some matrix and vector dimensions are of order $N-1$ in (35). Thus, for a number of Neumann steps r the number of operations needed to obtain $(\mathbb{1}+A_T)^{-1}\left(F^{10,01}\tilde{\mathbf{x}}_{01} - \tilde{\mathbf{x}}_{10}\right)$ is ca. $6rMV + 3rN + MV + N$, and to get the solution for the three vectors $\tilde{\mathbf{a}}_{00}^{-}$, $\tilde{\mathbf{a}}_{10}$ and $\tilde{\mathbf{a}}_{01}$ around $6rMV + 4MV + 3rN + 3N$ operations are necessary.

A direct inversion of a system of $3N$ equations with LDL^T factorization takes $\frac{(3N)^3}{3} = 9N^3$ operations [33]. In the case of a matrix multiplication for the whole $3N$ system, the matrix-vector multiplication takes $12N^2 - N$, avoiding the zeroes terms. A general iterative conjugate gradient algorithm (not optimized for this particular system) requires $30rN + r\left(12N^2 - N\right)$ operations for the solution of a $3N$ system of equations (see, e.g., [33] (10.2.16)). With preconditioning, an additional $3N$ matrix-vector multiplication for the right hand side and one additional $3N$ matrix-vector multiplication in each iteration are considered. The operation count results for each of the aforementioned solution algorithms are summarized in Table 1, as a function of the number of iterations r. The expressions shown in Table 1 are plotted in Figure 2. It is important to remark that the conjugate gradient operation count shown in this work corresponds to a generic CG algorithm, not to EGLib, which is specifically optimized for this particular system, leading to a lower computational load. As can be seen, the performance of the present algorithm (see orange lines) is better than the direct method. With the first iteration $r = 1$, the direct algorithm is slower than MuTLib algorithm for any number of species. For higher levels of iteration $r = 2$ and $r = 3$, direct method (blue lines) is better for small numbers of species, under 10. The operation count of MuTLib is slightly better than a generic conjugate gradient algorithm for small numbers of species and slightly worse for big numbers of species. However, the operation count of MuTLib with the recommended iteration level $r = 1$, is better than conjugate gradient for $r \geq 2$ for any number of species. On the other hand Figure 2 shows that the performance of MuTLib is better than a generic preconditioned conjugate gradient regardless of iteration level and number of species.

Algorithm	Number of operations
MuTLib algorithm	$12rN^2+8N^2-3rN-N$
LDL^T	$9N^3$
Conjugate gradient	$12rN^2+29rN$
Preconditioned conjugate gradient	$30rN^2+18N^2+26rN-3N$

Table 1: Number of operations needed to solve the transport system for a N species system for several iterative algorithms as a function of the number of iterations r.

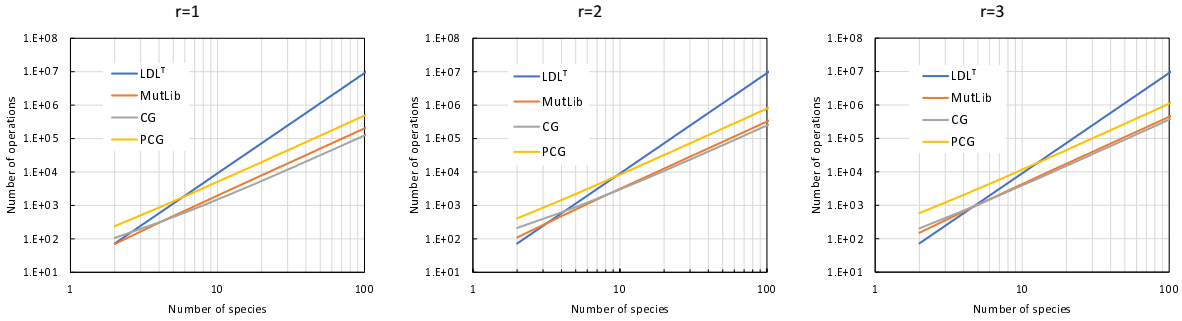

Figure 2: Operation count needed to solve the transport system for N species according to MuTLib, direct method LDT^T, iterative conjugate gradient (CG) and preconditioned conjugate gradient (PCG) as a function of the number of species for numbers of iterations $r=1$, 2, 3.

4. Numerical applications

The performance of the present approximate method is illustrated below in two particular cases of interest in combustion: a hydrogen premixed flame and a methane counterflow diffusion flame. We will focus on the accuracy of the results for the thermal diffusion fluxes D_{Ti} and partial thermal conductivity λ' vs. number of terms included in the iterative algorithm. To this end the package Chemkin with full multicomponent transport description (including Soret transport) has been used to determine the mole fraction and temperature profiles as a function of position in each flame configuration. Thus, the transport properties in the mixture are computed by Chemkin according to KTG [8] and provide the rigorous results for D_{Ti} and λ' as functions of position (termed $D_{Ti}\,(\text{exact KTG})$ and $\lambda'\,(\text{exact KTG})$ below). Then, based on the mole fraction and temperature profiles provided by Chemkin, the thermal diffusion coefficients D_{Ti} and partial thermal conductivity λ' are re-calculated according to the present iterative algorithm (Section 3, Eq. (37)) and the corresponding results (termed $D_{Ti}\,(\text{approximate model})$ and $\lambda'\,(\text{approximate model})$ below) are compared to the corresponding rigorous KTG values. To this end we define the absolute error in D_{Ti} and λ' as

$$\begin{aligned} \Delta D_{Ti} &= |D_{Ti}\,(\text{approximate model}) - D_{Ti}\,(\text{exact KTG})| \\ \Delta\lambda' &= |\lambda'\,(\text{approximate model}) - \lambda'\,(\text{exact KTG})| \end{aligned} \tag{40}$$

and will base our accuracy analysis in terms of the maximal absolute errors as a function of position, normalized by the maximal value of each corresponding rigorous KTG magnitude

$$\begin{aligned} \varepsilon_i &= \frac{\max\left(\Delta D_{Ti}\right)}{\max|D_{Ti}\,(\text{exact KTG})|} \\ \varepsilon_{\lambda'} &= \frac{\max\left(\Delta\lambda'\right)}{\max|\lambda'\,(\text{exact KTG})|} \end{aligned} \tag{41}$$

The same accuracy analysis will be also performed with the thermal diffusion fluxes and partial thermal conductivity computed by means of the mixture averaged approximation (Appendix A from additional material), and the corresponding normalized errors ε_i and $\varepsilon_{\lambda'}$ are also shown.

As explained in Section 3, the calculation of the thermal diffusion coefficients and partial thermal conductivity involves the calculation of the Fick diffusion coefficients. Hence, to focus on the accuracy of the Neumann series used for the inversion of the new sub-matrix $\mathbb{1}+A_T$ (Eq. (35)), in the results shown below the calculation of the Fick diffusion coefficients has been performed in an analytic way. As a consequence the inverse of matrix $\mathbb{1}+A$ is given by the corresponding exact result, which is equivalent to the leading order result of model 1+M in the optimized implementation shown in [27]. Thus, in the convergence

analysis shown below the normalized relative errors ε_i and $\varepsilon_{\lambda'}$ are shown as a function of the number of terms included in the Neumann series expansion used to calculate the inverse of the thermal diffusion sub-matrix $(\mathbb{1}+A_T)$ according to the present approximate algorithm (i.e., the maximal *finite* value considered for index r in Eq. (23)).

4.1. Results for premixed hydrogen flames

We consider a uni-dimensional hydrogen flame deflagration in air at 1atm and 300K as a function of the equivalence ratio ϕ, with chemical kinetics described by the seven-step combustion mechanism [34]. As a consequence only 8 species are present, numbered according to: H2, O2, H2O, O, OH, H, HO2, N2, with nitrogen as the reference species. As a particular case, Fig. 3 (major species) and Fig. 4 (radicals) show the results found for each chemical species as a function of position in a stoichiometric ($\phi = 1$) premixed hydrogen flame. Figures 3(a), 4(a) show the mole fraction and temperature profiles. Figures 3(b) and 4(b) show the thermal diffusion coefficients as a function of position for different algorithm approximations and mixture averaged. Figures 3(c), 4(c) show the relative errors found for different MuTLib algorithm approximations, mixture averaged and the available EGLib approximation. As can be seen in Figs. 3(c), 4(c), the convergence rate of the present algorithm is remarkable, yielding results which are quite accurate including only the first order term ($r = 1$) in the Neumann series expansion (Eq. (23)). On the other hand, Figs. 3(c), 4(c) also show that the mixture averaged approximation is quite inaccurate in this particular case (errors of MA approximation are out of range in Figs. 3(c), 4(c)). This result could be expected, since the mixture averaged approximation is a good approximation only in the dilute limit. Regarding the accuracy of EGLib, although for some species (H2, O, OH, H) the differences are almost as good as the MuTLib approximation for $r = 2$, the results for O2, H2O, HO2 and N2 with EGLib are similar to the MuTLib approximation for $r = 1$.

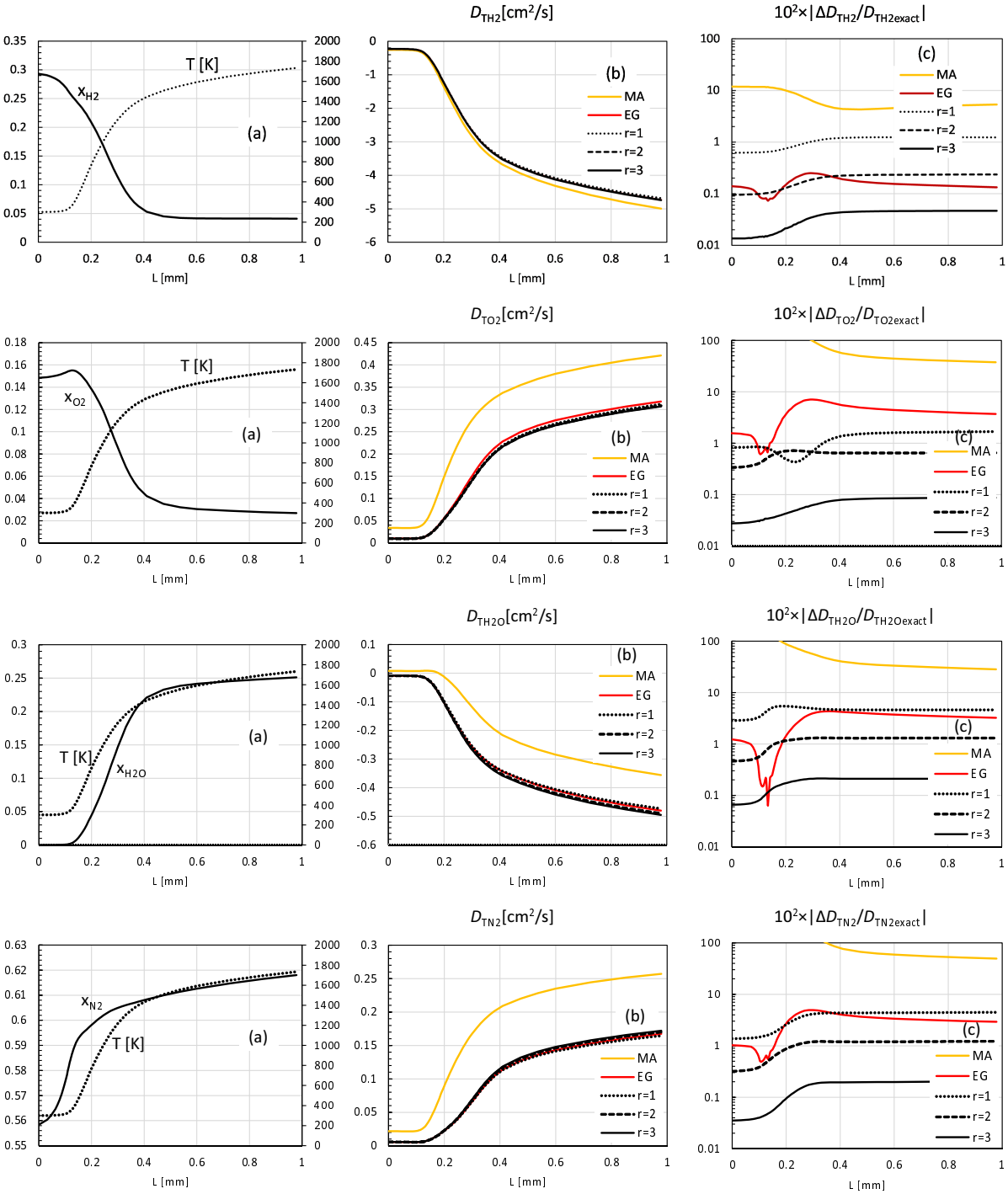

Figure 3: Results for the major species in a stoichiometric ($\phi = 1$) premixed hydrogen flame vs. distance L. Left column (a): mole fraction and temperature profiles. Center column (b): thermal diffusion coefficients. Right column (c): thermal diffusion coefficients percentage errors. The results for D_{Ti} (b) and $10^2 \times |\Delta D_{Ti}/D_{Tiexact}|$ (c) are shown for several maximal values of index r considered in the truncated Neumann series expansion (Eq. (23)). The results for D_{Ti} (b) using the mixture averaged (MA) approximation are shown in yellow lines. The results for $10^2 \times |\Delta D_{Ti}/D_{Tiexact}|$ (c) using the EGLib (EG) $r = 3$ approximation are also shown using red lines.

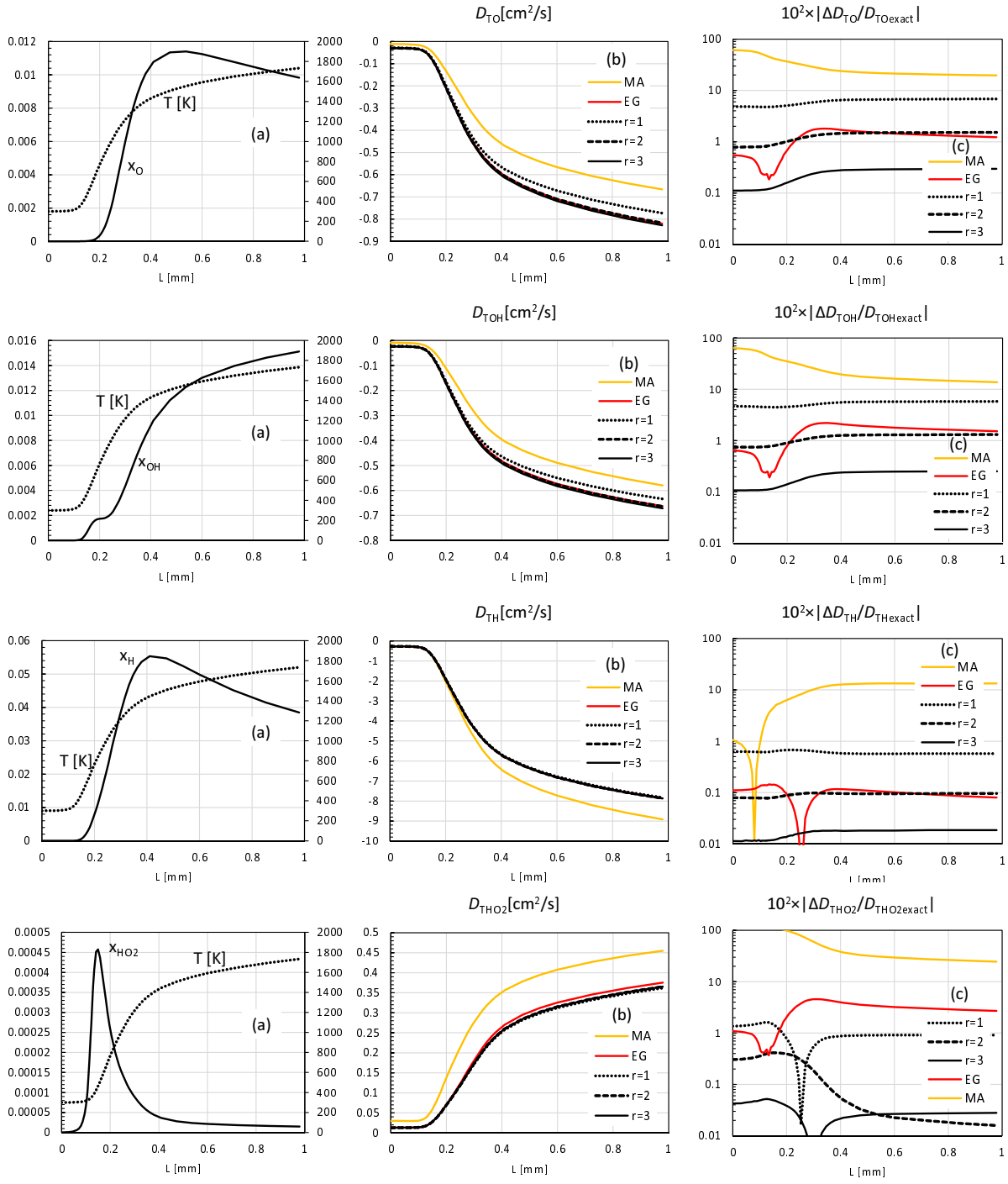

Figure 4: Results for the intermediate species in a stoichiometric ($\phi = 1$) premixed hydrogen flame vs. distance L. Left column (a): mole fraction and temperature profiles. Center column (b): thermal diffusion coefficients. Right column (c): thermal diffusion coefficients percentage errors. The results for D_{Ti} (b) and $10^2 \times |^{\Delta D_{Ti}}/_{D_{Tiexact}}|$ (c) are shown for several maximal values of index r considered in the truncated Neumann series expansion (Eq. (23)). The results for D_{Ti} (b) using the mixture averaged (MA) approximation are shown in yellow lines. The results for $10^2 \times |^{\Delta D_{Ti}}/_{D_{Tiexact}}|$ (c) using the EGLib (EG) $r = 3$ approximation are also shown using red lines..

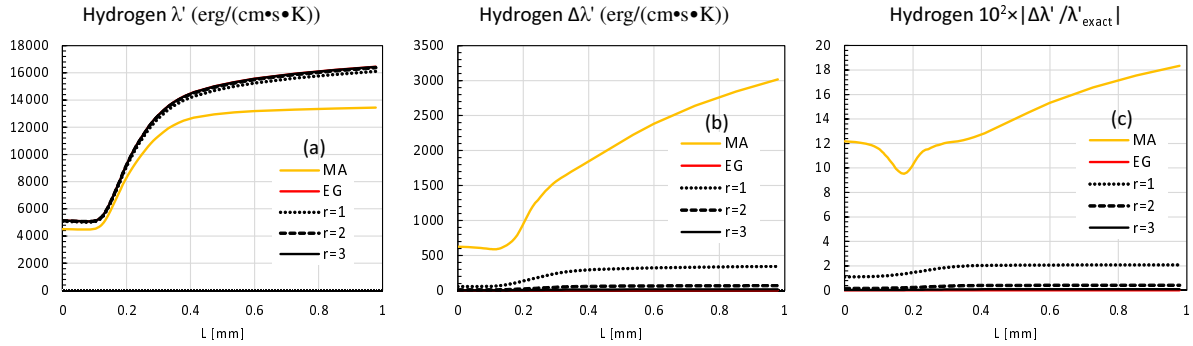

Figure 5: Partial thermal conductivity in a stoichiometric ($\phi = 1$) premixed hydrogen flame vs. distance L. Left column (a): partial thermal conductivity values. Center column (b): partial thermal conductivity absolute errors . Right column (c): partial thermal conductivity percentage errors. The results are shown for several maximal values of index r considered in the truncated Neumann series expansion (Eq. (23)). The results using the mixture averaged (MA) approximation are shown in yellow lines. The results using the EGLib (EG) $r = 3$ approximation are also shown using red lines.

Figure (5) shows the results for the partial thermal conductivity. As in the former results, we find that the mixture averaged approximation is again quite inaccurate, while the EGLib results for three conjugate gradient iterations (with preconditioning in the last one) provide almost the exact values. In this case the results found with the present MuTLib algorithm are not as accurate as those found using EGLib. However, the accuracy of MuTLib for the partial thermal conductivity is around 2% for $r = 1$, which is remarkably accurate.
Figures 6, 7 and 8 show the normalized relative errors ε_i and $\varepsilon_{\lambda'}$ (Eq. (41)) vs. maximal value of r in Eq. (23) found according to the present algorithm, as well as the mixture averaged approximation. In the present analysis we have considered values of the equivalence ratio ϕ covering the whole range between the lean-flame (Fig. 6) and the rich-flame (Fig. 8) limits, while the results for a stoichiometric flame are shown in Fig. 7. As can be seen, the present algorithm is quite accurate and has very fast convergence rate. In all the cases considered the first order term of the Neumann series (Eq. (23)) provides maximal relative errors of order 10% (often lower than 10%), and this error decreases by ca. an order of magnitude with each new term included in the truncated Neumann series.
Figures 6, 7 and 8 also show that the present iterative algorithm is considerably more accurate than the mixture averaged approximation, even if the Neumann series is truncated at the first order term ($r = 1$). Regarding the comparison of relative errors among the different species, it should be noted that the present definition of the normalized relative errors ε_i (Eq. (41)) penalizes those species with lowest thermal diffusion coefficients. Therefore the species H2 and H have lower relative errors in Figs. 6, 7, 8 according to

both, the present model and the mixture averaged approximation.

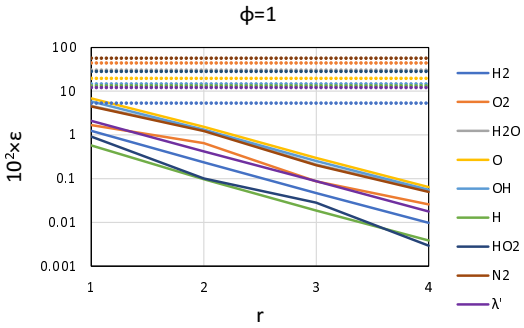

Figure 7: Relative errors found vs. r for stoichiometric flames. Dotted horizontal lines = Mixture Averaged Model. Continuous lines= present algorithm.

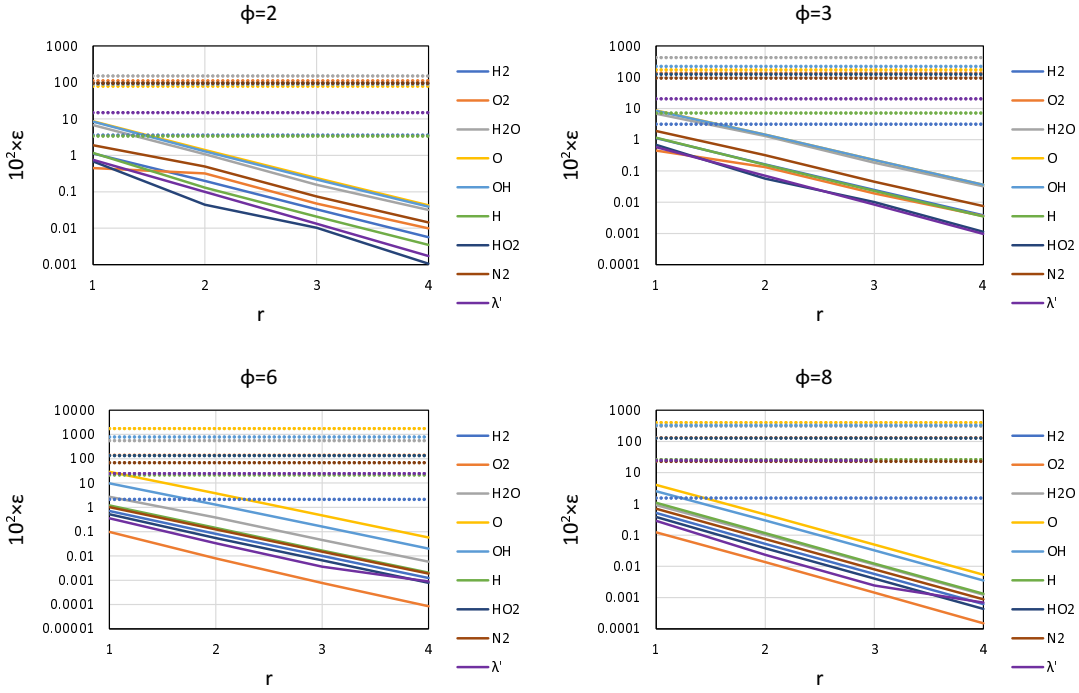

Figure 8: Relative errors found vs. r for rich flames. Dotted horizontal lines = Mixture Averaged Model. Continuous lines = present algorithm.

We recall that an apparent linear decrease of ε_i and $\varepsilon_{\lambda'}$ vs. r in the semi-log Figs. 6, 7,

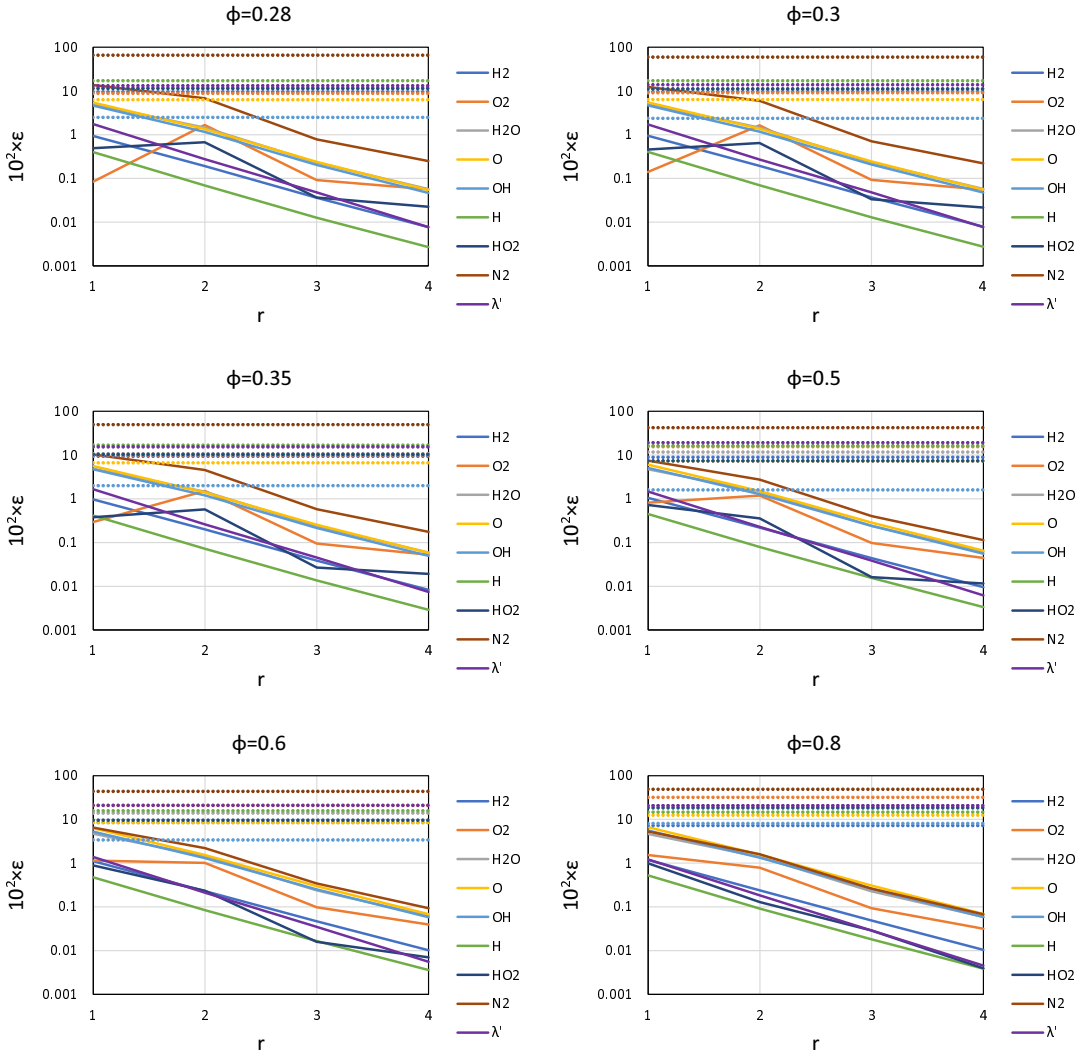

Figure 6: Normalized relative errors ε_i and $\varepsilon_{\lambda'}$ (Eq. (41)) found vs. maximal r considered in the truncated Neumann series (Eq. (23)) for lean hydrogen premixed flames. Dotted horizontal lines: corresponding results found with the mixture averaged approximation.

8 corresponds to an exponential convergence rate of the present algorithm. Hence, the results for the normalized relative errors ε_i and $\varepsilon_{\lambda'}$ in Figs. 6, 7, 8 seem to fit to the general exponential decrease formula

$$\varepsilon = \varepsilon_1 e^{-\alpha(r-1)} \tag{42}$$

where the prefactor ε_1 provides the accuracy of the present model truncated at the first order term ($r = 1$), while the exponent α provides the convergence rate. The results of this fit are shown in Fig. 9 for each particular chemical species vs. the equivalence ratio. The most relevant feature of the present algorithm that can be seen in Fig. 9 is an overall relative error of order 10% at the first order term and an exponential convergence rate with a relative error reduction close to an order of magnitude for each new term included in the truncated Neumann expansion (Eq. (23)). We also remark that the accuracy and convergence rate of the present algorithm is not as dependent on equivalence ratio as it happens to Model 1 and Model $1+M$ of [26] for the Fick diffusion fluxes. In the present algorithm this has been accomplished by means of the diagonal term scaling of the KTG system (Eqs. (25–26)).

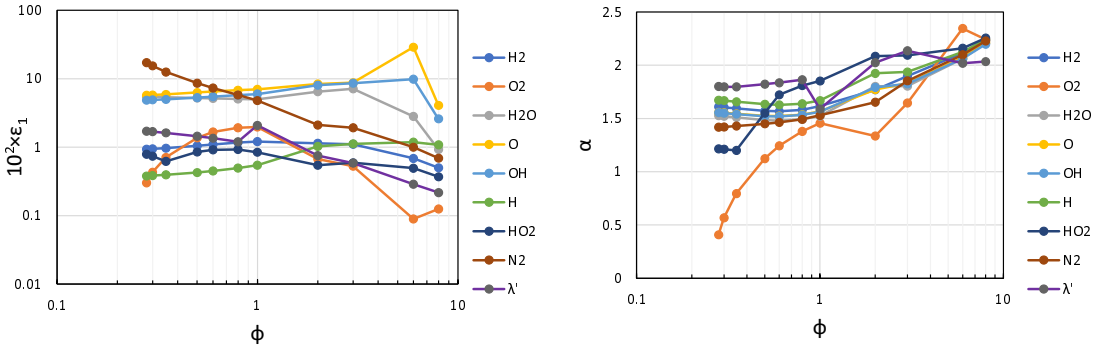

Figure 9: Results for maximal relative error ε_i fitted to the formula $\varepsilon = \varepsilon_1 e^{-\alpha(r-1)}$ vs. ϕ for all species. Left: $10^2 \times$ first order term error ε_1. Right: exponent α.

4.2. Results for methane counterflow diffusion flames

To show the performance of the present algorithm in the case of a diffusion flame we consider a counterflow diffusion flame configuration. Two counterflow jets are simulated, with methane as fuel at $x = 0$mm and air as oxidizer at $x = 20$mm. The initial compositions are summarized in Table 2. The chemical mechanism of [35] is used, involving 58 species and 270 reactions. The stagnation point is fixed at $x = 10$mm with strain rate $a = 100\text{s}^{-1}$. The Chemkin boundary conditions must be iterated to simulate the desired condition and to obtain the molar fractions and temperature as a function of distance. The basis of the steady flame model used in this section is described in reference [36].

	Fuel	Oxidizer
Temperature	$T = 320\text{K}$	$T = 1350\text{K}$
Mole fractions	$x_{\text{CH4}} = 0.33$ $x_{\text{O2}} = 0.15$ $x_{\text{N2}} = 0.52$	$x_{\text{H2O}} = 0.15$ $x_{\text{O2}} = 0.12$ $x_{\text{N2}} = 0.73$

Table 2: Conditions of temperature and species mole fractions of fuel and oxidizer.

Figure 10 shows the results for the species with higher thermal diffusion flux, CH4, O, H2O and N2. According to the present results we find that in this case the first order term of the present iterative algorithm is already more accurate than both, mixture averaged approximation and EGLib package.

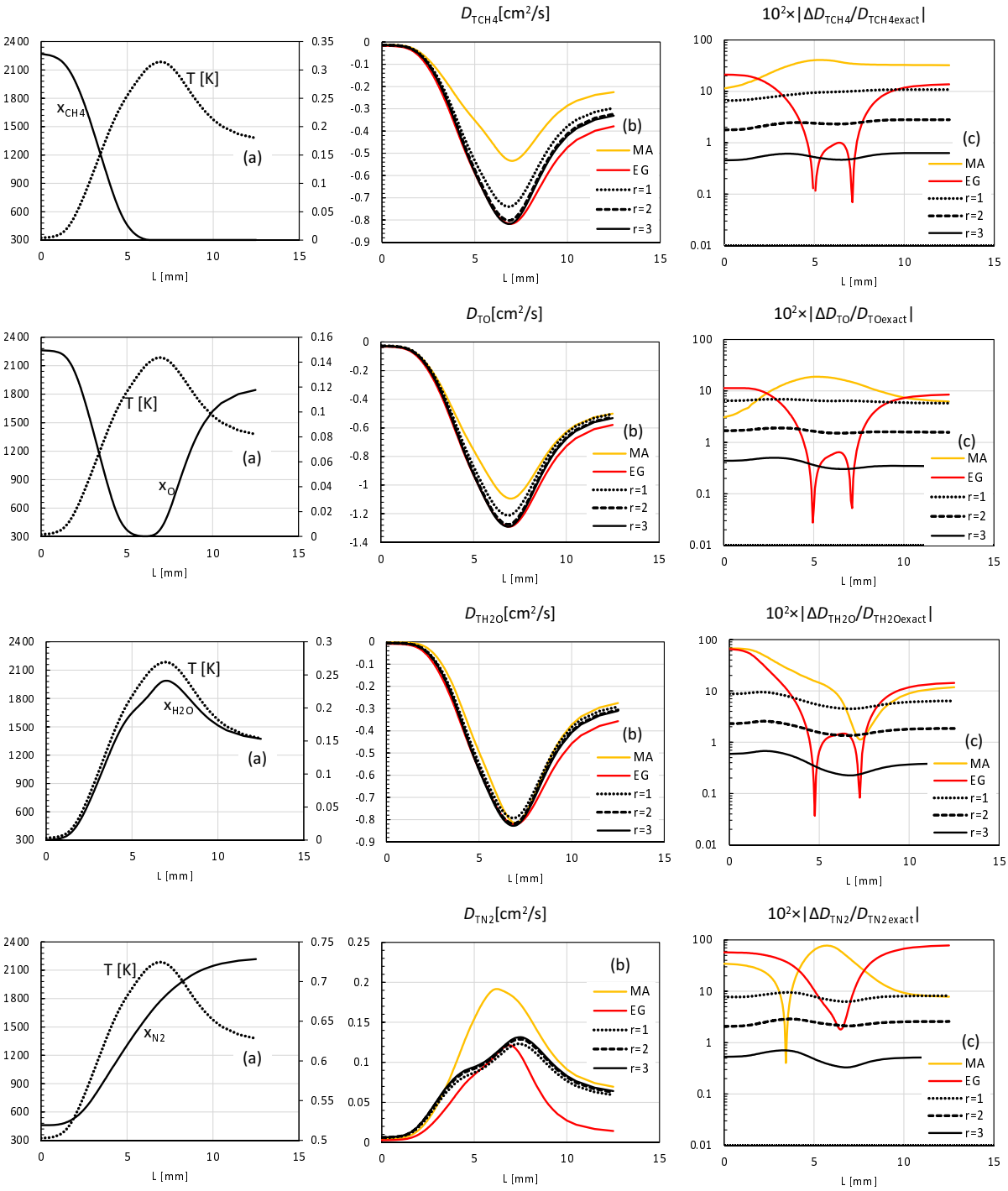

Figure 10: Results vs. axial distance L for the major species CH4, O, H2O and N2; mole fraction x and temperature T (a), thermal diffusion coefficients (b) and thermal diffusion coefficients percentage error (c) as compared to exact (KTG) values for different approximation terms, mixture averaged approximation (yellow lines) and EGLib with $r = 3$ (red lines).

Figure 11 presents the results for the species O2, H2, CO2 and CO with meaningful thermal diffusion flux. The accuracy increases with the number of iterations considered in the truncated Neumann series expansion (Eq. (23)), as could be expected. As can be seen, the shape of the curves is similar in all the cases, which could also be expected since the thermal diffusion fluxes are proportional to the temperature gradient in all the cases.

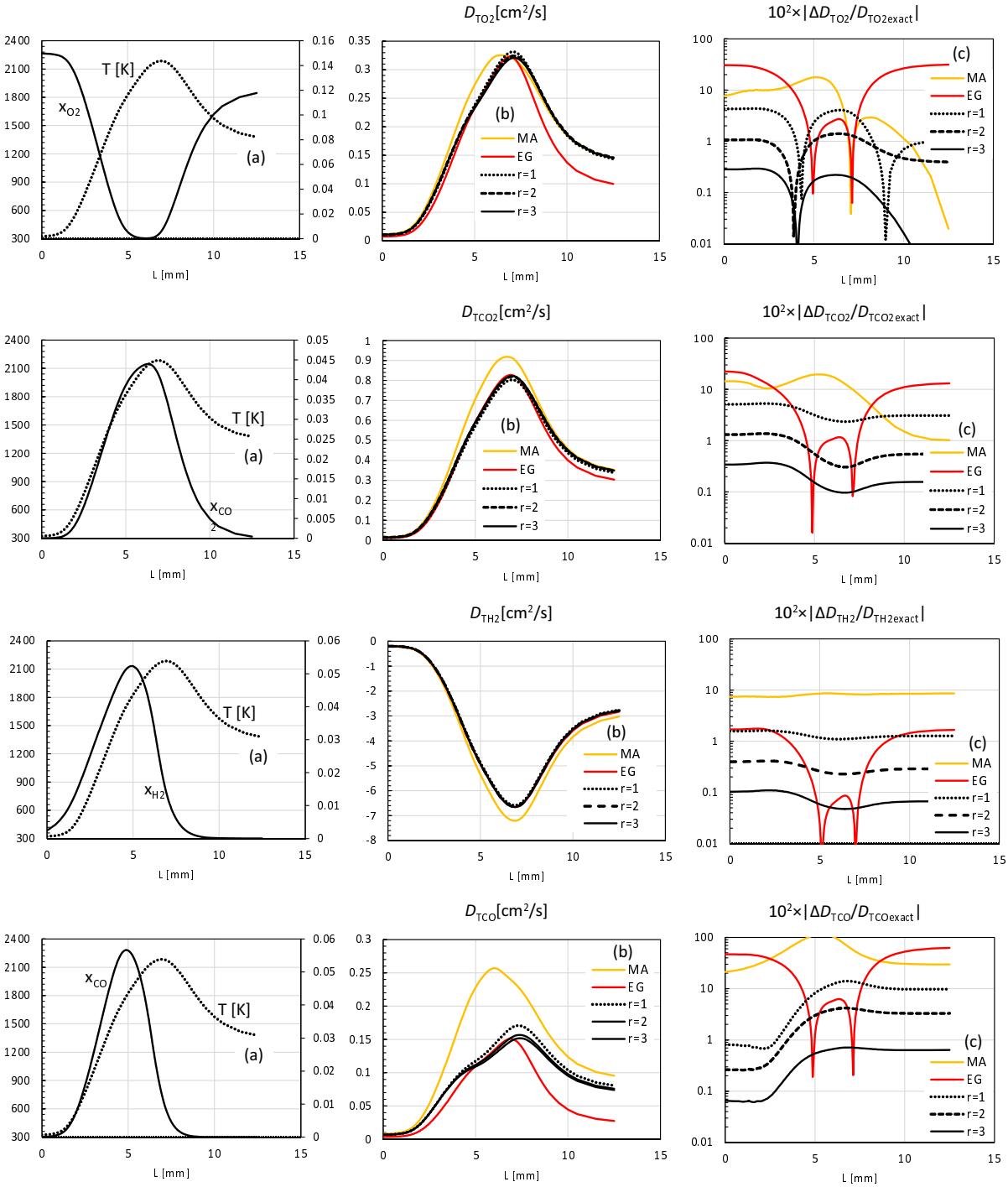

Figure 11: Results for species O2, CO2, H2 and CO vs. axial distance L; mole fraction x and temperature T (a), thermal diffusion coefficients (b) and thermal diffusion coefficients percentage error (c) as compared to exact (KTG) values for different approximation terms, mixture averaged approximation (yellow lines) and EGLib with $r = 3$ (red lines).

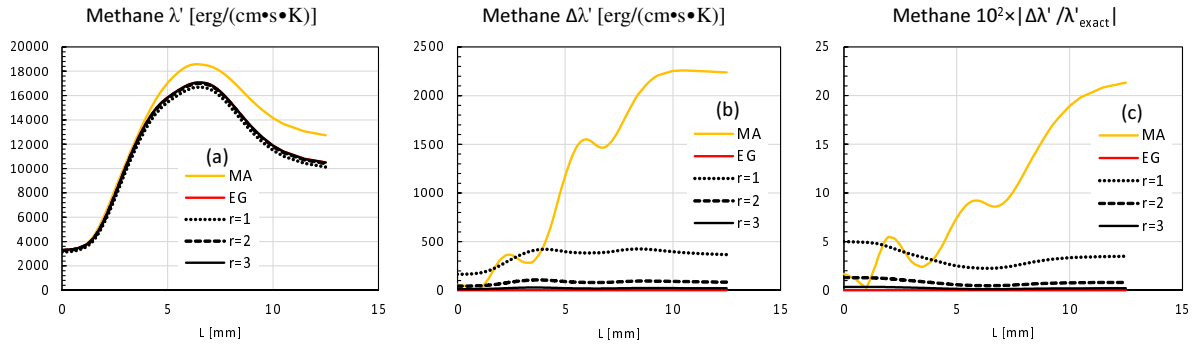

Figure 12: Partial thermal conductivity in a methane diffusion flame vs. distance L. Left column (a): partial thermal conductivity values. Center column (b): partial thermal conductivity absolute errors . Right column (c): partial thermal conductivity percentage errors. The results are shown for several maximal values of index r considered in the truncated Neumann series expansion. The results using the mixture averaged (MA) approximation are shown in yellow lines. The results using the EGLib (EG) $r = 3$ approximation are also shown using red lines.

Figure (12) shows the results for the partial thermal conductivity. As can be seen, the mixture averaged approximation is very inaccurate, while EGLib (which includes three preconditioned conjugate gradient iterations) provides results which are indistinguishable from the exact values. As can be seen in Fig. (12), the results found with the present algorithm (with $r = 1,2,3$) are not as accurate as those found with EGLib. However, the relative errors found with MuTLib including only the first Neumann series iteration (r=1) is less than 5% (remaining around 3% in most of the integration domain), which is a remarkable result.

Figure 13 shows the relative errors for the species CH4, O, H2O, N2, O2, CO2, H2, CO and the thermal conductivity for the present iterative algorithm and mixture averaged. As in the case of the premixed hydrogen flame, the error decays exponentially and therefore the error curves look linear in semi-logarithmic scales. As can be seen in Fig. 13, the relative errors may be fitted to the exponential decrease formula Eq. (42), in a similar way as it was done in the case of a premixed hydrogen flame. The results from this fit show that ε_1 values range from 1.11% (H2) to 14.8% (N2). In the case of the convergence rate exponent α, the results are very similar for all species, ranging between 1.35 (λ') and 1.53 (H2). Hence, the accuracy and convergence rate of the present algorithm in the methane counterflow diffusion flame configuration is comparable to the corresponding results found in the premixed hydrogen flame configuration.

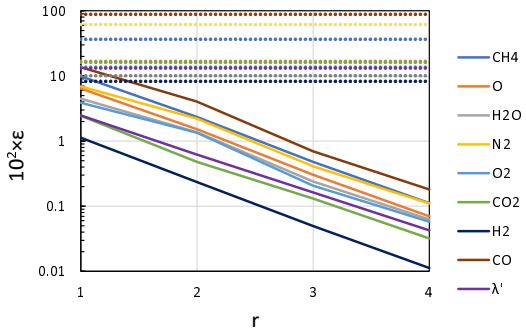

Figure 13: Normalized relative errors ε_i and $\varepsilon_{\lambda'}$ (Eq. (41)) found vs. maximal r considered in the truncated Neumann series (Eq. (23)) for methane counterflow diffusion flames. Dotted horizontal lines: corresponding results found with the mixture averaged approximation.

5. Conclusions

A new iterative algorithm for an efficient and accurate multicomponent thermal diffusion coefficients and partial thermal conductivity calculation based on the kinetic theory of gases (KTG) is described. The central idea leading to this new algorithm lies in using the proper scaled parameters and a detailed examination of the different matrices that must be inverted in the resultant system of linear equations, derived from the KTG. The terms involving inelastic collisions and relaxation times for the internal degrees of freedom in polyatomic gases are considered and the resonant exchange of rotational energy is also accounted for in the case of polar gases, in addition to the classical Chapman-Enskog expressions. Thus, the present model considers the same physical effects included in the full multicomponent transport description considered in the Chemkin package.

In the case of a multicomponent mixture with N chemical species, the proposed algorithm makes use of the $N-1 \times N-1$ matrix inversion needed for the calculation of the Fick's diffusion coefficients, a problem addressed in Model 1 and Model $1+M$ of reference [26]. Based on these results, the calculation of the thermal diffusion coefficients involves a new $2N \times 2N$ (or $(N+P) \times (N+P)$, where P is the number of non monoatomic molecules) system of equations, which is diagonally dominant. As a consequence, scaling this system by the corresponding diagonal terms allows for a fast convergence rate iterative algorithm, based on the Neumann series.

The efficiency, accuracy and convergence rate of this new algorithm have been successfully analyzed. The number of operations implied in the present algorithm is analyzed, and is shown to be lower than well known iterative and direct methods. The results are compared against the mixture averaged approximation and the transport package developed by Ern and Giovangigli, EGLib, for two examples of practical interest: a premixed hydrogen

flame and a methane counterflow diffusion flame. We show that the proposed new iterative algorithm at the first order term is already more accurate than the mixture average approximation in all the cases considered. On the other hand, regarding the thermal diffusion coefficients it is shown that the first order term of the present algorithm is comparable to the results based on the EGLib library including three conjugate gradient iterations (the iteration level provided in the library) for the premixed hydrogen flame, and much more accurate for the methane diffusion flame. However, regarding the partial thermal conductivity EGLib is considerably more accurate after three conjugate gradient iterations than the present algorithm (which provides results with relative errors of ca. 3%). Regarding convergence rate beyond the first order term, we find that each new term in the new iterative algorithm provides a relative error reduction in thermal diffusion fluxes close to an order of magnitude, making it a very accurate and efficient algorithm.
As a general conclusion the present algorithm for the thermal diffusion coefficients and partial thermal conductivity, together with the results shown in [26] for the Fick's diffusion coefficients, provide an extremely efficient and accurate method for the calculation of molecular mass transport coefficients in mixtures with large numbers of components, which will be of interest for the numerical simulation of detailed combustion mechanisms involving large numbers of chemical species. The aforementioned new algorithms have been implemented in the C++ software library package MuTLib (Multicomponent Transport Library) for the transport properties calculations in third party applications, which is available as additional material of this publication.

Nomenclature

A	perturbation matrix for Fick's diffusion calculation
A_T	perturbation matrix for thermal diffusion calculation
D	Fick difussion coefficient
D_T	thermal difussion coefficient
$\mathscr{D}$	binary diffusion coefficient
$\mathbf{j_T}$	thermal diffusion flux
k_B	Boltzmann constant
n	number density
p	pressure

T	absolute temperature
$\mathbf{v}$	mixture hydrodynamic velocity (barycentric)
x	mole fraction
y	mass fraction

Abbreviations

DNS	Direct Numerical Simulation
EGLib	Ern Giovangigli Library
KTG	Kinetic Theory of Gases
MA	Mixture Averaged
MuTLib	Multicomponent Transport Library

Greek Symbols

ϵ	well depth Lennard Jones potential
λ	thermal conductivity
λ'	partial thermal conductivity
ϕ	equivalence ratio
ρ	mass density

Subscripts

(n)	Chapman-Enskog approximation index

Superscripts

(n)	Chapman-Enskog approximation index

Acknowledgments

Supported by Ministerio de Ciencia e Innovación (#PID2019-108592RB-C44). It is a pleasure to acknowledge many fruitful discussions with B. Naud and D. Fernández-Galisteo at CIEMAT and P.L. García-Ybarra and J.L. Castillo at UNED. In particular the authors would like to thank B. Naud for his help with the expressions simplification in Section 3.1 and D. Fernández-Galisteo for his help with the hydrogen seven step mechanism Chemkin file generation. Thanks also to A. Ern for providing EGLib code and his further support on the library setup.

References

[1] F. A. Williams. *Combustion Theory*. CRC Press, second edition, 1994.

[2] R. B. Bird, W. E. Stewart, and E. N. Lightfoot. *Transport Phenomena*. Wiley, New York NY, second edition, 2007.

[3] D. E. Rosner. *Transport Processes in Chemically Reacting Flow Systems*. DOVER, Mineola NY, 2000.

[4] S. Chapman and T. G. Cowling. *The Mathematical Theory of Non-Uniform Gases*. Cambridge University Press, Cambridge UK, third edition, 1985.

[5] J. O. Hirschfelder, C. F. Curtiss, and R. B. Bird. *The Molecular Theory of Gases and Liquids*. Wiley, New York NY, second edition, 1964.

[6] J. H. Ferziger and H. G. Kaper. *Mathematical Theory of Transport Processes in Gases*. North-Holland, 1972.

[7] C. S. Wang-Chang and G. E. Uhlenbeck. Transport phenomena in polyatomic gases. Technical report, University of Michigan, 1959.

[8] L. Monchick and E. A. Mason. Transport properties of polar gases. *The Journal of Chemical Physics*, 35(5):1676–1697, 1961.

[9] E. A. Mason and L. Monchick. Heat conductivity of polyatomic and polar gases. *The Journal of Chemical Physics*, 36(6):1622–1639, 1962.

[10] L. Monchick, K. S. Yun, and E. A. Mason. Formal kinetic theory of transport phenomena in polyatomic gas mixtures. *The Journal of Chemical Physics*, 39(3):654–669, 1963.

[11] Faizan Habib Vance, Philip de Goey, and Jeroen A. van Oijen. The effect of thermal diffusion on stabilization of premixed flames. *Combustion and Flame*, 216:45–57, 2020.

[12] J. Schlup and G. Blanquart. Validation of a mixture-averaged thermal diffusion model for premixed lean hydrogen flames. *Combustion Theory and Modelling*, 22(2):264–290, 2018.

[13] J. De Charentenay and A. Ern. Multicomponent transport impact on turbulent premixed H2/O2 flames. *Combustion Theory and Modelling*, 6(3):439–462, 2002.

[14] C. Bruno, V. Sankarana, H. Kollab, and J. H. Chen. Impact of multi-component diffusion in turbulent combustion using direct numerical simulations. *Combustion and Flame*, 162:4313–4330, 2015.

[15] G. Dixon-Lewis. Flame structure and flame reaction kinetics II. Transport phenomena in multicomponent systems. *Proceedings of the Royal Society of London Series. A-Mathematical and Physical Sciences*, 307(1488):111–135, 1968.

[16] W. W. Jones and J. P. Boris. An algorithm for multispecies diffusion fluxes. *Computers and Chemistry*, 5(2-3):139–146, 1981.

[17] E. S. Oran and J. P. Boris. Detailed modeling of combustion systems. *Progress in Energy and Combustion Science*, 7(1):1–72, 1981.

[18] A. Ern and V. Giovangigli. Impact of detailed multicomponent transport on planar and counterflow hydrogen/air and methane/air flames. *Combustion Science and Technology*, 149(1):157–181, 1999.

[19] V. Giovangigli. *Multicomponent Flow Modeling*. Birkhäuser, Boston, 1999.

[20] V. Giovangigli. Multicomponent transport in laminar flames. *Proceedings of the Combustion Institute*, 35(1):625–637, 2015.

[21] V. Giovangigli. Convergent iterative methods for multicomponent diffusion. *IMPACT of Computing in Science and Engineering*, 3(3):244–276, 1991.

[22] A. Ern and V. Giovangigli. Projected iterative algorithms with application to multicomponent transport. *Linear Algebra and Its Applications*, 250:289–315, 1997.

[23] A. Ern and V. Giovangigli. *Multicomponent Transport Algorithms*. Springer - Verlag, 1994.

[24] Nancy J. Brown, Lucas A.J. Bastien, and Phillip N. Price. Transport properties for combustion modeling. *Progress in Energy and Combustion Science*, 37(5):565–582, 2011.

[25] Y. Xin, W. Liang, W. Liu, T. Lu, and C. K. Law. A reduced multicomponent diffusion model. *Combustion and Flame*, 162(1):68–74, 2015.

[26] M. Arias-Zugasti, P. L. García-Ybarra, and J. L. Castillo. Efficient calculation of multicomponent diffusion fluxes based on kinetic theory. *Combustion and Flame*, 163:540–556, 2016.

[27] B. Naud and M. Arias-Zugasti. Accurate multicomponent Fick diffusion at a lower cost than mixture-averaged approximation: Validation in steady and unsteady counterflow flamelets. *Combustion and Flame*, 219:120–128, 2020.

[28] P. L. Garcia-Ybarra, C. Nicoli, and P. Clavin. Soret and dilution effects on premixed flames. *Combustion Science and Technology*, 42(1-2):87–109, 1984.

[29] Oscar Córdoba. *Analysis of iterative algorithms based on KTG for transport properties of multicomponent mixtures*. PhD thesis, UNED, 2022.

[30] K. Chen. *Matrix Preconditioning Techniques and Applications*. Cambridge University Press, Cambridge UK, 2005.

[31] A. Ern and V. Giovangigli. Eglib: A general-purpose fortran library for multicomponent transport property evaluation.

[32] Robert J. Kee. Theory Manual C HEMKIN ® Software. *Design*, (May):1–273, 2004.

[33] Gene H. Golub and Charles F. Van Loan. *Matrix Computation*. The Johns Hopkins University Press, third edition, 1996.

[34] D. Fernández-Galisteo, A. L. Sánchez, A. Liñán, and F. A. Williams. One-step reduced kinetics for lean hydrogen-air deflagration. *Combustion and Flame*, 156(5):985–996, 2009.

[35] Combustion Research Group at UC San Diego. The San Diego mechanism. Chemical-Kinetic Mechanisms for Combustion Applications. https://web.eng.ucsd.edu/mae/groups/combustion/mechanism.html.

[36] R. J. Kee, J. A. Miller, G. H. Evans, and G. Dixon-Lewis. A computational model of the structure and extinction of strained, opposed flow, premixed methane-air flames. *Symposium (International) on Combustion*, 22(1):1479–1494, 1989.